Desalination and Water Treatment
www.deswater.com
doi: 10.5004/dwt.2023.30064

312 (2023) 119–131
November

Removal of amoxicillin and lead from aqueous solutions using immobilized nanoparticles: green synthesis, characterization, and kinetic study

Haneen Salih Hadi, Ziad Tark Abd Ali*

Department of Environmental Engineering, College of Engineering, University of Baghdad/Iraq,
emails: z.teach2000@yahoo.com (Z.T. Abd Ali), Hanin.Hadi2111p@coeng.uobaghdad.edu.iq (H.S. Hadi)

Received 8 August 2023; Accepted 6 October 2023

ABSTRACT

In this study, the nanoparticles (Fe/Zn) were immobilized using sand to produce S-Fe/Zn nanocomposite in an eco-friendly approach using *Eucalyptus* leaf extract as an antioxidant instead of harmful chemicals, the prepared S-Fe/Zn was then employed for the removal of amoxicillin (AMX) and lead (Pb(II)) from aqueous solutions in batch mode. This study involved characterizing the nanocomposite using various tests such as X-ray diffraction, scanning electron microscopy, energy-dispersive X-ray spectroscopy, Fourier-transform infrared spectroscopy, Brunauer–Emmett–Teller surface area, and transmission electron microscopy, in addition, the factors that influenced the contaminants' removal process which achieved the highest removal presence of 90% and 85% for Pb(II) and AMX, respectively, were investigated. The results indicated that the Freundlich and pseudo-second-order models provided a better fit to the experimental data. This suggests that the sorption of AMX and Pb(II) onto the S-Fe/Zn nanocomposite followed a multilayer sorption process, and the rate-limiting step was predominantly controlled by chemisorption. Overall, this study demonstrates the effectiveness of utilizing green nanocomposites (S-Fe/Zn) created from agricultural waste for the removal of contaminants from aqueous solutions. Finally, employing environmentally friendly synthesis techniques and utilizing agricultural waste materials, this approach offers a sustainable and innovative solution for wastewater treatment.

Keywords: Characterization; Amoxicillin; Lead ions; Nanocomposite; Kinetic

1. Introduction

Environmental pollution caused by a mixture of organic chemicals and heavy metals is a significant concern worldwide, these pollutants can originate from various sources such as industrial activities, agricultural practices, improper waste disposal, and more, therefore, ensuring a clean and healthy environment for human well-being requires effective methods for removing these contaminants [1,2]. Heavy elements like lead (Pb(II)) and antibiotics such as amoxicillin (AMX) pose significant threats to both the environment and human health. Antibiotics such as amoxicillin (AMX) are vital in the treatment of bacterial infections, benefiting humans, animals, poultry, and fish. However, their use should be responsible and guided by appropriate prescription practices to mitigate the risks associated with antibiotic resistance [3]. Lead (Pb(II)) is indeed recognized as one of the most harmful heavy metals in the environment, and its consumption through the food chain can have severe health consequences. Lead exposure can occur through various sources such as contaminated water, soil, dust, and certain consumer products. When lead enters the body, it can affect multiple organs and systems, leading to a range of health issues [4]. The removal of toxic heavy metal ions from the environment is a significant challenge. A removal process must be simple, effective and inexpensive. a due to their

* Corresponding author.

detrimental effects on ecosystems and human health [5]. Therefore, developing ways to treat or remove these pollutants is one of the important things that must be taken care of to create a clean environment.

Nano-zero-valent iron (nZVI) technology has shown promising results in the field of remediation [6]. nZVI refers to nanoscale particles of zerovalent iron that exhibit high reactivity and can effectively degrade or immobilize various contaminants in water and soil environments [7,8]. However, nZVI particles do have some limitations, including quick aggregation, poor stability, and difficulties in separating them from the reactants after the remediation process [9]. Emulsifying nZVI particles, doping with additional metals, applying chemical stabilizers to the surface, and adding support materials are all strategies commonly used to improve the performance of nZVI particles in remediation applications. These approaches can enhance the stability, reactivity, and separation of nZVI particles, leading to more effective contaminant removal [10]. The addition of metal dopants in bimetallic nZVI particles serves as catalysts and can enhance the ability of nZVI particles to remove contaminants. Bimetallic nZVI particles combine the reactivity of zerovalent iron with the catalytic properties of the additional metal, leading to improved contaminant degradation or immobilization [11]. The dopant metal stabilizes the system by preventing the oxidation of airborne particles in addition to acting as a catalyst. Additionally, it assists in reducing the activation energy, enhancing the reduction energy [12]. The increased reactivity resulting from H_2 production near the nZVI surface enhances the degradation kinetics of contaminants. It promotes the transfer of electrons and facilitates the reduction of pollutants, particularly organic compounds and certain heavy metals. The enhanced reactivity also allows for a wider range of contaminants to be effectively treated using bimetallic nZVI particles [13]. By utilizing Zn(II) as a dopant metal and employing green synthesis techniques through using agricultural waste extract as safe antioxidants instead of chemical materials that have negative effects on the environment, the researchers have contributed to the development of more sustainable and environmentally friendly approaches to remediation. This not only expands the knowledge base but also paves the way for the future development of safe and effective nanoparticle-based remediation technologies [14]. The utilization of agricultural waste for biosynthesis of nanoparticles is a potential solution that aligns with the principles of sustainability and environmental consciousness. Agricultural waste, such as plant residues, husks, peels, or extracts derived from them, contain a variety of bio-organics, such as polyphenols, proteins, polysaccharides, and enzymes, which can serve as reducing agents, stabilizers, or capping agents for the synthesis of nanoparticles [15]. In this work, *Eucalyptus* leaves have been employed as a valuable source of green antioxidants instead of harmful chemicals. It contains mainly flavonoids, which are a group of water-soluble organic compounds produced by the secondary metabolism of plants and belong to the class of polyphenols, they play a crucial role in protecting against oxidative stress and damage caused by free radicals. The main flavonoids present are catechins, isorhamnetin, luteolin, kaempferol, phloretin, and quercetin [16]. These flavonoids offer various health benefits and have potential applications in different industries. For example, *Eucalyptus* leaf extract can be used in textile dyeing to impart new functionalities to textile fibers. By incorporating *Eucalyptus* extract into cotton fabrics, it is possible to enhance their properties, such as imparting anti-UV and antimicrobial properties [17]. Furthermore, *Eucalyptus* leaf extract has shown promise in mitigating the presence of toxic metabolites (cyanotoxins) in water [18]. By utilizing *Eucalyptus* leaf extract, it is possible to control and reduce the proliferation of cyanobacteria in aquatic environments, thus ensuring the optimal state of water quality [19]. In addition to textile and water-related applications, *Eucalyptus* leaf extract has been explored in other fields as well. It has been studied for its potential pharmaceutical uses and has found applications in the cosmetic and food industries [20]. The diverse range of beneficial compounds present in *Eucalyptus* leaves, especially polyphenols compounds, makes them a subject of increasing interest and research in various industries [21,22].

Through a survey of the previous literature, there are many works deal with synthesizing nanoparticles using a dopant metals like Cu, Ag, Pt, Ni, Pd, and Pb that are doped into nZVI [23–28], and other used harmful and dangerous chemical compounds like borohydride [29,30] but no one of these works used Zn(II) as a dopant metal as used in this work for the first time.

The main objective of the present study is to develop a novel sorbent capable of the removal of organic (AMX) and inorganic (Pb(II)) contaminants. The utilization of Zn with nZVI supported on the sand to produce S-Fe/Zn nanocomposite through a green synthesis method by using *Eucalyptus* leaf extract represents a unique approach for the removal of AMX and Pb(II) from aqueous solutions. The combination of green synthesis through the utilization of agricultural waste, using Zn(II) as a dopant metal with nZVI to produce S-Fe/Zn nanocomposite, and the removal of organic (AMX) and inorganic (Pb(II)) contaminants, enriched the importance to this work for the development of environmentally sustainable solutions that used nanotechnology for water treatment.

2. Materials and methods

2.1. Materials

The sand(s), quartz type, was used as a supported and immobilized matrix, it was purchased from the local market (Al-Nawafth Company, Al-Najaf City, Iraq), with specific properties such as initial porosity = 0.45, particle size range = 0.3–0.6 mm, and specific gravity = 1.36. The lead sulfate ($PbSO_4$), ferric chloride ($FeCl_3$), zinc chloride ($ZnCl_2$), and absolute ethanol (99.9%) were purchased from the local market (Honeywell Specialty Chemicals, Germany), while amoxicillin ($C_{16}H_{19}FN_3O_5S$) from Samarra Pharmaceutical Factory, Iraq. All chemicals and reagents were of analytical grade.

2.2. Preparation of contaminated aqueous solutions

The contaminated solutions of Pb(II) and AMX with a concentration of 1,000 mg/L were prepared by dissolving 1.598 and 1 g of lead sulfate and amoxicillin, respectively, in 1 L of distilled water. The required contaminant

concentration is obtained through the dilution process. The pH adjustment of the prepared solutions was performed using 0.1 M HCl (hydrochloric acid) or NaOH (sodium hydroxide) solutions to achieve the desired pH for the experimental conditions.

2.3. Synthesis of S-Fe/Zn nanocomposite

2.3.1. Preparation of Eucalyptus leaf extract as green antioxidant

To prepare the *Eucalyptus* leaf extract using ethanol for the green synthesis of the S-Fe/Zn nanocomposite, firstly the *Eucalyptus* leaves were cleaned with tap water to remove any impurities, then they were carefully ground into a fine powder using a grinder, where the powder formula facilitates the extraction of desired compounds or enhance their release. The *Eucalyptus* leaf powder was dried for 48 h at a temperature of 65°C in an oven, this drying process helps remove moisture from the leaf and prepares them for extraction. The dried *Eucalyptus* leaf powder (15% weight/volume) was mixed with 100% ethanol in a shaking incubator, the mixture was allowed to shake for 24 h, allowing the ethanol to extract the bioactive compounds from the *Eucalyptus* leaf, then the mixture of *Eucalyptus* leaf and ethanol was filtered using Whatman No.1 filter paper. The filtration step helps remove any solid particles or residue from the extract, leaving behind a clear liquid. Finally, the filtered solution, known as the *Eucalyptus* leaf extract, was collected in a container and stored at a temperature of 20°C for future use in the green synthesis process.

2.3.2. Coating sand with Fe/Zn nanoparticles

The green synthesis of the S-Fe/Pb nanocomposite was carried out according to the study of Abdulhusain and Abd Ali [1], this method involves the following steps: (1) Mixing sand (S) with $FeCl_3$ solution, where 30 g of sand was mixed with 150 mL of a 0.3 M $FeCl_3$ solution, the mixture was placed on an orbital shaker and shaken for 30 min to ensure thorough mixing of the $FeCl_3$ solution and sand, (2) Drying of Fe-coated sand, where the $FeCl_3$-coated sand obtained from the previous step was dried overnight in an 80°C vacuum oven, drying process helps remove any moisture and ensures the stability of the coated sand, (3) Addition of *Eucalyptus* leaf extract, where the dried $FeCl_3$-coated sand was mixed with *Eucalyptus* leaf extract (15% concentration). As the *Eucalyptus* leaf extract was added, the color of the mixture changed from golden yellow to black, the color change indicates the reduction of iron ions to zero-valent iron, resulting in the formation of small-sized nanoparticles, (4) Mixing and reaction, where the mixture of $FeCl_3$-coated sand and *Eucalyptus* leaf extract was maintained on an orbital shaker at room temperature for 30 min to ensure uniform mixing, after that, 150 mL of a 0.3 M $ZnCl_2$ solution was added to the mixture, the shaking time was increased to 1 h to allow sufficient reaction time for the formation of the S-Fe/Zn nanocomposite, (5) Filtration, washing, and drying, where the prepared S-Fe/Zn nanocomposite was filtered to separate the solid composite from the reaction mixture, the filtered composite was washed three times with 100% ethanol to remove any impurities or residual reactants, after washing, the composite was dried in an 80°C vacuum oven to remove any remaining solvent and ensure complete drying, and (6) Storage, where the prepared S-Fe/Zn nanocomposite was stored in a closed container for use in the experiments of this study. The schematic diagram of the green synthesis of S-Fe/Zn nanocomposite is illustrated in Fig. 1.

2.4. Characterization of S-Fe/Zn nanocomposite

The prepared S-Fe/Zn nanocomposite was thoroughly characterized before its use in the experiments. The characterization was conducted at the College of Science, University of Tehran, Iran, and subsequently at the College of Science, University of Kashan, Iran. The characterization methods used are as follows: X-ray diffraction (XRD) analysis was performed to determine the crystal structure and phase composition of the nanocomposite, scanning electron microscopy (SEM) was employed to investigate the surface morphology and particle size of the nanoparticle, energy-dispersive X-ray spectroscopy (EDX) carried out to determine the elemental composition of the nanocomposite, Fourier-transform infrared (FTIR) spectroscopy performed to identify the functional groups present in the nanocomposite, Brunauer–Emmett–Teller surface area analysis conducted to determine the specific surface area and porosity of the nanocomposite, and finally transmission electron microscopy (TEM) analysis examined to clarify the morphology of the sand and S-Fe/Zn nanocomposite using a Morgagni 270-D transmission electron microscope, (Hillsboro, Oregon, USA) and an 80.0 kV speed voltage. To estimate the TEM, by dabbing the sample solution onto the Formvar® coated grids, the aim is to disperse the sample material thinly and evenly across the grid surface.

2.5. Batch experiments

The batch mode experiments were conducted to determine the optimum conditions for the removal of AMX and Pb(II) contaminants using the prepared S-Fe/Zn nanocomposite. Several variables were considered, including contact time, pH of the initial solution, agitation rate, concentration of the initial contaminants, and dosage of the S-Fe/Zn nanocomposite. The following procedure was used in the experimental work: each 250 mL flask was first filled with 50 mL of the AMX and Pb(II) solutions at a concentration of 50 mg/L, and then 0.2 g of the prepared nanocomposite was added. After being stirred for 3 h at 200 rpm, all of the flasks containing the adsorbent, as well as the AMX and Pb(II) contaminant solutions, were filtered to separate the clear contaminant solution from the remaining solid material, the residual untreated quantity of the AMX and Pb(II) present in the solution was specified using 10 mL samples drawn from the filtered solution. Pb(II) was examined using atomic absorption spectroscopy (AAS), and the AMX was evaluated using UV-Visible spectroscopy. To guarantee the accuracy of the findings, every sample was re-examined three times. At various pH ranges (for AMX pH = 2–12 and for Pb(II) pH = 2–6). Based on the various initial concentrations of the contaminants (C_o, 50–250 mg/L), the sorption was calculated using a variety doses (0.06–1 g/50 mL), time range from 0 to 180 min. To evaluate the removal percentage (R%)

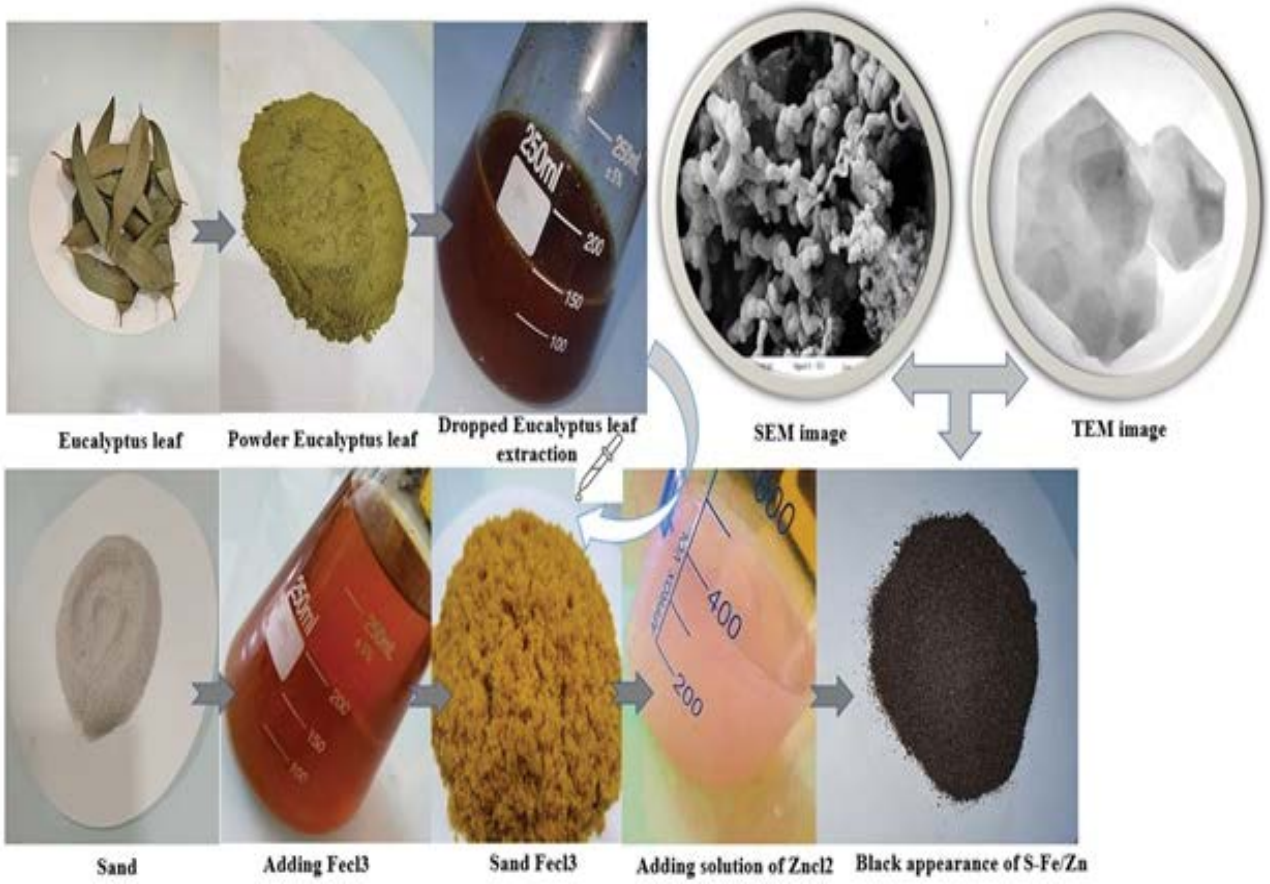

Fig. 1. Schematic diagram of the green synthesis of S-Fe/Zn nanocomposite.

and the number of contaminants retained in the solid phase (q_e), Eqs. (1) and (2) were used, as referenced by the study of Abdulhusain and Abd Ali [31]:

$$R\% = \frac{C_0 - C_e}{C_0} \times 100 \quad (1)$$

$$q_e = \frac{C_0 - C_e}{m} V \quad (2)$$

where C_o is the initial concentration of contaminants (mg/L) in the flask, C_e is the equilibrium concentration of contaminants (mg/L) in the flask, V is the volume of the solution in the flask (L), m is the mass of the S-Fe/Pb nanocomposite in the flask (g).

2.6. Isotherm models

In this study, two isotherm models were used to describe the sorption data:

2.6.1. Freundlich isotherm model

Freundlich isotherm model is commonly used to describe sorption on non-homogeneous surfaces with multilayer sorption. It is an empirical equation that relates the equilibrium concentration of a sorbate in a sorbent to the sorbate concentration in the bulk solution. The formula for the Freundlich model [32,33]:

$$q_e = K_F C_e^{1/n} \quad (3)$$

where q_e is the amount of sorbate adsorbed per unit mass of sorbent (sorption capacity), K_F is the Freundlich constant related to the adsorption capacity of the sorbent, C_e is the equilibrium concentration of the sorbate in the bulk solution, and n is the Freundlich exponent that describes the intensity of adsorption. The value of n indicates the favorability of sorption, where $n > 1$ represents favorable adsorption, $n = 1$ represents linear adsorption, and $0 < n < 1$ suggests less favorable or weak adsorption.

2.6.2. Langmuir isotherm model

Langmuir isotherm model is a widely used isotherm model in adsorption studies, particularly for homogenous surfaces and monolayer sorption. It describes the relationship between the concentration of adsorbate (gas or solute) in the bulk phase and the amount of adsorbate adsorbed onto the surface of an adsorbent material. The Langmuir model equation is typically given by the study of Abd Ali et al. [34,35]:

$$q_e = \frac{q_{\max} b C_e}{1 + b C_e} \quad (4)$$

where q_{max} which is the maximum amount of adsorbate that can be adsorbed per unit mass of the adsorbent (mg/g), The parameter "*b*" is usually is known as the Langmuir constant or equilibrium constant. In the Langmuir model, it is assumed that adsorption occurs on a homogenous surface, forming a monolayer of adsorbate molecules. The model assumes that the adsorption sites on the surface are identical and independent, and there is no interaction between the adsorbate molecules adsorbed on adjacent sites.

2.7. Kinetic models

There are several models that can be used to calculate the adsorption rate of solute particles in the sorption process [36]. Some commonly used models include:

2.7.1. Pseudo-first-order kinetic model

This model assumes that the sorption process follows first-order kinetics. The rate of sorption is proportional to the difference between the equilibrium sorption capacity and the amount of solute already adsorbed. The equation for the pseudo-first-order model is given by the study of Abd Ali et al. [37,38]:

$$\frac{dq}{dt} = k_1\left(q_e - q_t\right) \tag{5}$$

Eq. (5) is integrated to obtain Eq. (6):

$$q_t = q_e\left(1 - e^{-k_1 t}\right) \tag{6}$$

where dq/dt is the rate of sorption at time t, k_1 is the rate constant of the pseudo-first-order model, q_e is the equilibrium sorption capacity, q_t is the amount of solute adsorbed at time t.

2.7.2. Pseudo-second-order kinetic model

This model assumes that the sorption process follows second-order kinetics. The rate of sorption is proportional to the product of the difference between the equilibrium sorption capacity and the amount of solute already adsorbed, and the square of the remaining solute concentration. The equation for the pseudo-second-order model is [39,40]:

$$\frac{dq}{dt} = k_2\left(q_e - q_t\right)^2 \tag{7}$$

Eq. (7) is integrated to produce the next equation in nonlinear forms:

$$q_t = \frac{t}{\left(\frac{t}{k_2 q_e^2} + \frac{t}{q_t}\right)} \tag{8}$$

where dq/dt is the rate of sorption at time t, k_2 is the rate constant of the pseudo-second-order model, q_e is the equilibrium sorption capacity, q_t is the amount of solute adsorbed at time t.

2.7.3. Intraparticle diffusion model

This model considers that the sorption process involves intraparticle diffusion as a rate-determining step. The equation for the intraparticle diffusion model is given by the study of Du et al. [41]:

$$q_t - k_{int} \times t^{0.5} + C \tag{9}$$

where q_t is the amount of solute adsorbed at time t, k_{int} is the rate constant of the intraparticle diffusion model.

It is important to note that the choice of the appropriate kinetic model depends on the specific sorption system and experimental data. The selected model should provide the best fit to the experimental data and help determine the controlling factors of the sorption process, such as surface reactions, diffusion, or other phenomena.

3. Results and discussion

3.1. Characterization of the prepared nanocomposite (S-Fe/Zn)

The XRD analysis of the S-Fe/Zn nanocomposite before and after interaction with Pb(II) and AMX provides valuable information about its structural characteristics and changes that occur after interaction with the selected contaminants. The obtained XRD spectral data is presented in Fig. 2, which shows diffraction peaks at specific angles (2θ values) indicating the presence of certain crystalline phases. The diffraction peaks observed at 2θ = 42.82°, 50.21°, 60.35°, and 67.87°. According to the XRD spectrum-specific crystal planes, these prominent peaks suggest the successful formation of Fe/Zn nanoparticles on the sand surface, indicating the formation of the desired nanocomposite material (S-Fe/Zn). After interaction of prepared S-Fe/Zn with AMX, a significant decrease in the intensity of the peak at 2θ = 50.321° is observed. This decrease can be attributed to a redox reaction occurring between AMX and S-Fe/Zn, where the reaction between the organic molecules of AMX and the active sites on the S-Fe/Zn surface leads to changes in the crystallinity and structure, resulting decline in the intensity of the corresponding diffraction peak [42]. On the other hand, when S-Fe/Zn interacts with Pb(II), there is a decrease in the peak intensity specifically

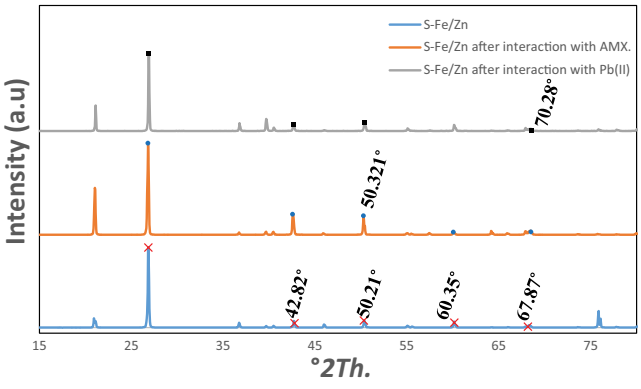

Fig. 2. X-ray diffraction test for S-Fe/Zn before and after interaction with AMX and Pb(II).

at 2θ = 70.28°. The sorption of Pb(II) alters the crystallinity and phase of the S-Fe/Zn material, leading to a change in the XRD pattern [43]. The differences observed in the XRD patterns for S-Fe/Zn before and after the interactions with Pb(II) and AMX suggest variations in the crystallinity, phase composition, and structure of the S-Fe/Zn composite due to the sorption processes. These changes in the XRD spectra provide insights into the interactions between the adsorbent (S-Fe/Zn) and the adsorbates (Pb(II) and AMX), and can help understand the mechanisms and transformations occurring during the sorption process.

The FTIR analysis of S-Fe/Zn, shown in Fig. 3, provides information about the functional groups and chemical bonds present in the nanocomposite. The analysis reveals specific peaks in the range of 400–4,000 cm^{-1}, indicating the presence of certain functional groups and their involvement in the sorption processes. The stretching vibrations of the O–H and C–H functional groups are observed as multiple peaks at 791.1; 3,791.3 and 1,082.8 cm^{-1}, the spectrophotometric images were studied, and the functional groups illustrated on the surface of the sorbent were recognized [44]. These peaks are attributed to the polyphenol content of the *Eucalyptus* leaf extract used in the synthesis of S-Fe/Zn [45]. The presence of these functional groups confirms the role of bio-organics in the leaf extract in promoting the accumulation of nanoparticles (Fe/Zn) on the sand surface. This observation is consistent with previous studies that utilized *Eucalyptus* leaf extracts for the production of metal nanoparticles. Furthermore, the FTIR spectrum supports the sorption of Pb(II) and AMX by S-Fe/Zn. Specific peaks at 3,851; 2,911.2; 1,070.3 and 801.2 cm^{-1} are attributed to the adsorbed AMX, indicating the presence of relevant functional groups involved in the sorption process [11]. Similarly, peaks at 3,442.4; 2,917.7; 1,634.6 and 1,084.7 cm^{-1} confirm the existence of sorbed Pb(II) on the surface of S-Fe/Zn. FTIR analysis results provide evidence of the adsorption of AMX and Pb(II) onto the surface of S-Fe/Zn and suggest the involvement of specific functional groups and chemical bonds in sorption interactions. Overall, the FTIR spectral analysis aided in understanding the chemical nature of S-Fe/Zn and provided insights into the functional groups responsible for the sorption processes involving AMX and Pb(II). It confirmed the role of bio-organics from the *Eucalyptus* leaf extract in the synthesis of S-Fe/Zn and their impact on the sorption behavior of the composite material.

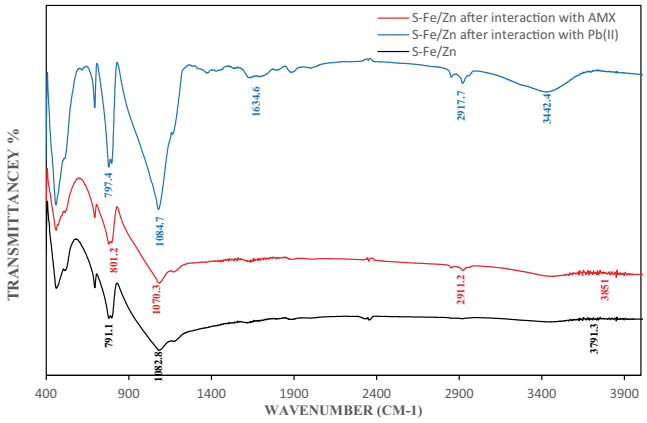

Fig. 3. Fourier-transform infrared spectroscopy test for S-Fe/Zn before and after interaction with AMX and Pb(II).

The surface area and pore volume of the manufactured nanocomposite (S-Fe/Zn) were determined using this analysis that illustrated that the surface area of the S-Fe/Zn was significantly higher compared to the sand alone, where the surface area was 6.2992 and 0.787 m^2/g for S-Fe/Zn and sand, respectively. Additionally, the pore volume of the sand increased from 0.0074298 to 0.030058 cm^3/g after being coated with the Fe/Zn nanoparticles. The increase in surface area and pore volume of S-Fe/Zn can be attributed to the coating of the sand surface with the nanoparticles (Fe/Zn) which led to increases in the available surface area for sorption, as the nanoparticles create additional active sites for interactions with particles of contaminants. This result aligns with the findings of other researchers, such as Abd Ali [34], who also observed an increase in surface area and pore volume when nanoparticles were coated on a substrate. The increased surface area and pore volume offer enhanced adsorption capacity and accessibility, making S-Fe/Zn more effective in sorption applications, providing a favorable environment for sorption processes, and further supporting the understanding of the impact of nanoparticle coatings on substrate properties.

The SEM images and EDX analysis provide valuable insights into the morphology and elemental composition of S and S-Fe/Zn, as depicted in Fig. 4. The SEM images reveal that the mean diameter of the nanoparticles (Fe/Zn) coated on the sand surface was 58.03 nm. The majority of the particles exhibit a spherical shape. This information indicates the size and morphology of the Fe/Zn nanoparticles formed on the sand surface. The spherical shape is often desired in nanoparticle synthesis as it offers a high surface area-to-volume ratio, which can enhance adsorption and reactivity. Furthermore, the EDX analysis of S-Fe/Zn verified the presence of both iron (Fe) and zinc (Zn) on the sand surface. The EDX analysis allowed for the identification and quantification of elemental composition. In this case, the presence of Fe and Zn confirms the successful coating of Fe/Zn nanoparticles onto the sand surface. The combination of SEM images and EDX analysis provides complementary information about the physical structure and elemental composition of S-Fe/Zn. This information contributed to the understanding of the characteristics and composition of S-Fe/Zn, which is important for assessing its potential applications in various fields, particularly in sorption processes.

The TEM images of S and S-Fe/Zn nanocomposite provided further insights into the structure and morphology of the samples, as illustrated in Fig. 5. In Fig. 5a, the TEM image of S showed that the sand particles appeared as a single piece without any small parts constituent. This confirms that the sand particle is not coated with any additional material or nanoparticles, and it did not exhibit any significant morphological changes under the TEM imaging. On the other hand, in Fig. 5b, the TEM image of S-Fe/Zn nanocomposite revealed the presence of small intermittent pieces or discrete particles that are different from the single, uncoated sand particles observed in Fig. 5a. These discrete particles indicate the successful deposition of Fe/Zn nanoparticles on the sand surface. The formation of these discrete particles

signified the presence of the Fe/Zn nanoparticles and their attachment to the sand particles. The TEM images provided direct visual evidence of the morphological changes that occurred when the Fe/Zn nanoparticles are introduced to the sand surface. The presence of discrete particles in the S-Fe/Zn nanocomposite confirms the successful coating of Fe/Zn nanoparticles onto the sand surface, demonstrating the modification of the sand morphology. Overall, the TEM images in Fig. 5 supported the successful deposition of Fe/Zn nanoparticles on the sand surface, as demonstrated by the presence of discrete particles in the S-Fe/Zn composite and the absence of such particles in the sand alone.

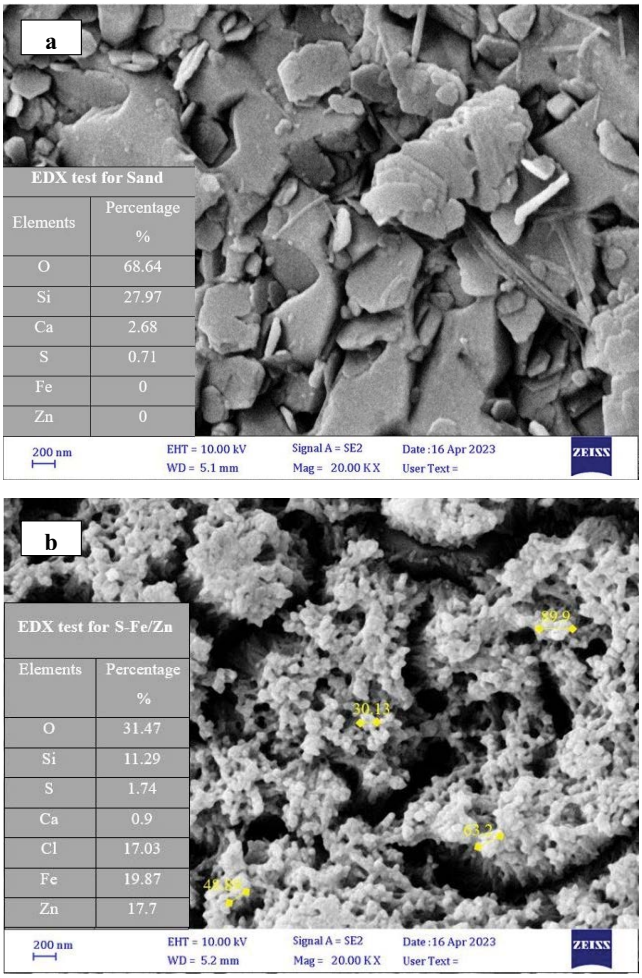

Fig. 4. Scanning electron microscopy images and energy-dispersive X-ray spectroscopy test for (a) sand and (b) S-Fe/Zn.

3.2. Impact of operational conditions in batch mode

3.2.1. Contact time

Determining the equilibrium time is crucial for understanding the optimal duration required for achieving maximum removal efficiency of the target contaminants (AMX and Pb(II)). The experimental conditions and results are illustrated in Fig. 6a. The interaction time between the S-Fe/Zn and the contaminants varied from 5 to 180 min. The results showed that the highest removal percent of AMX (55%) and Pb(II) (76%) were predominantly achieved at 120 min. The significant increase in removal percentage over time can be attributed to the availability and accessibility to the active sites on the S-Fe/Zn for sorbing the AMX and Pb(II) contaminants. Initially, all active sites were available for sorption, resulting in a higher removal percent, then with the passage of time, the available sorption sites became saturated or reduced, so the sorption rate gradually decreased. This reduction in the sorption rate becomes more pronounced after 120 min for AMX and Pb(II) [46]. After this time value, the elimination percent did not exhibit significant changes up to 180 min, indicating that the system had approached equilibrium. Therefore, 120 min represents the optimal times required to achieve the equilibrium state for the removal of AMX and Pb(II).

3.2.2. Effect of initial pH of the aqueous solution

The pH of the aqueous solution plays a crucial role in the removal of AMX and Pb(II), and it was taken into account in this study. Tests were conducted using fixed initial pH values, specifically 2–12 for AMX and 2–6 for Pb(II), with the operating conditions as illustrated in Fig. 6b. The results

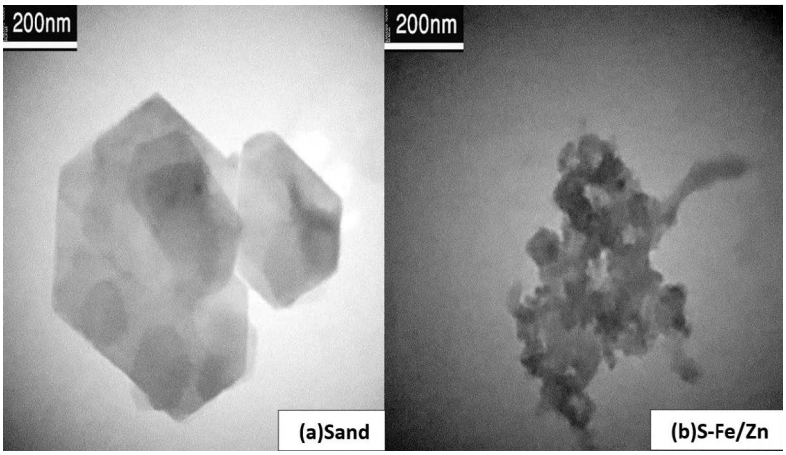

Fig. 5. Transmission electron microscopy images for (a) sand, and (b) S-Fe/Zn.

indicate that the removal percentages of the contaminants increased as the initial pH value increased from 2 up to 11 and 6 for AMX and Pb(II), respectively. These values represent the optimal points where the highest removal percentages of 73% for AMX and 76% for Pb(II) were achieved. However, beyond these pH values, the removal percentages decreased or remain constant with further increases in the initial pH value. This observation aligns with the findings of other studies, such as Abd Ali and Ismail [38], which also reported a similar trend. This behavior can be explained as follows: within the experimental pH range of 2–11 for AMX and 2–6 for Pb(II), increasing the pH values led to an increase in the removal percentages. This is because increasing the pH decreases the obstacles to the attraction between the contaminants and the active sites of the adsorbent (S-Fe/Zn) by repulsion, which is controlled by the protonation of the nanocomposite [10]. However, beyond the optimal pH range, the removal pattern differed. The removal percentages decreased with further increases in the pH values, up to 12 for AMX and 7 for Pb(II). This can be attributed to the ionization of hydroxyl groups [47], where at higher pH values, the increased ionization of hydroxyl groups on the adsorbent surface can lead to a decrease in the adsorption efficiency. Considering the pH of the aqueous domain is crucial in this study, as it directly influences the interaction between the contaminants and the adsorbent material. By understanding the pH dependence, optimal pH ranges can be determined to achieve maximum removal efficiencies. These findings contribute to the overall understanding of the adsorption process using S-Fe/Zn nanocomposite and aid in the design of effective adsorption strategies for AMX and Pb(II) removal.

3.2.3. Effect of agitation speed

The effect of agitation speed on the removal of Pb(II) and AMX was investigated by varying the speed from 0 to 250 rpm while keeping the other parameters constant at their optimal values. The results are shown in Fig. 6c. Initially, without any agitation (0 rpm), approximately 5% of AMX and 10% of Pb(II) were removed even before the system was subjected to shaking. This initial removal may be attributed to the natural settling or weak interactions between the contaminants and the sorbent surface. As the agitation speed increased from 0 to 200 rpm, the removal percentages of both AMX and Pb(II) increased significantly. At 200 rpm, the highest removal percentages of 73% for AMX and 76% for Pb(II) were achieved. This suggests that increasing the agitation speed enhances the distribution of the contaminants on the surface of the sorbent (S-Fe/Zn), leading to improved contact between the sorbate solution and the active sites available for sorption [38]. The increased contact and improved mass transfer facilitate the successful transfer of the contaminants from the solution to the sorbent sites, resulting in higher removal efficiencies. However, when the agitation speed was further increased to 250 rpm, there was no significant increase in the removal percentages. This suggests that the optimal agitation speed for achieving the maximum removal efficiency of AMX and Pb(II) is 200 rpm. The explanation for these results lies in the fact that increasing the agitation speed promotes better mixing and distribution of the contaminants, ensuring effective contact between the sorbate solution and the active sites of the sorbent material. However, beyond a certain speed (200 rpm in this case), the additional increase in agitation speed does not provide any substantial benefits in terms of improved removal percentages. Based on these findings, an agitation speed of 200 rpm was selected as the optimal value for subsequent experiments, as it resulted in the highest removal percentages for AMX and Pb(II).

3.2.4. Effect of initial concentration

To investigate the effect of different initial concentrations (C_0) of AMX and Pb(II) on the removal percentage, additional experiments were conducted. The initial concentrations of AMX and Pb(II) varied from 50 to 250 mg/L while keeping other operating conditions constant, as depicted in Fig. 6d. The results clearly demonstrate a significant decrease in the removal percentages for AMX and Pb(II) as their initial concentrations (C_0) were increased. This decline in removal rates can be attributed to the saturation of adsorbent sites with the molecules of the pollutants. As the initial concentration increases, the number of pollutant molecules in the solution becomes higher, leading to a higher chance of occupying all available sorption sites on the adsorbent surface. Consequently, the adsorbent becomes saturated, resulting in a decrease in the removal efficiency [39,40]. Based on the findings of this experiment, the optimal beginning concentration that achieved the highest removal percent was determined, which was 50 mg/L. At this value of initial concentration, the adsorbent sites are not rapidly saturated, allowing for more effective sorption and higher removal percentages. It is important to consider the initial concentration of contaminants in practical applications, as it directly affects the sorption capacity and efficiency of the adsorbent material. By identifying the optimal beginning concentration, it becomes possible to design treatment processes that maximize removal while minimizing the required adsorbent dosage and operating costs.

3.2.5. Effect of S-Fe/Zn dosage

In order to evaluate the dependence of AMX and Pb(II) removal on the dosage of S-Fe/Zn composite, an experiment was conducted using different dosages ranging from 0.05 to 1 g/50 mL. Each dosage was added and continuously mixed with 50 mL of aqueous contaminant solution, under the operating conditions specified in Fig. 6e. The results obtained from this experiment indicate that using 0.5 g/50 mL of S-Fe/Zn composite resulted in the removal of 65% of AMX and 70% of Pb(II). However, an increase in the nanocomposite dosage to 1 g/50 mL led to a significant enhancement in the removal percent of 85% and 90% for AMX and Pb(II), respectively. This improvement can be attributed to the increased amount of sorbent material, which provides a greater number of active sites for sorption [48]. It is worth noting that further increasing the dosage above 1 g/50 mL does not considerably affect the removal percentage. This can be explained by the stability of the contaminant concentration remaining in the aqueous phase, indicating that the sorbent has reached its saturation point, at which any increase in the sorbent dosage does not lead to a significant increase in

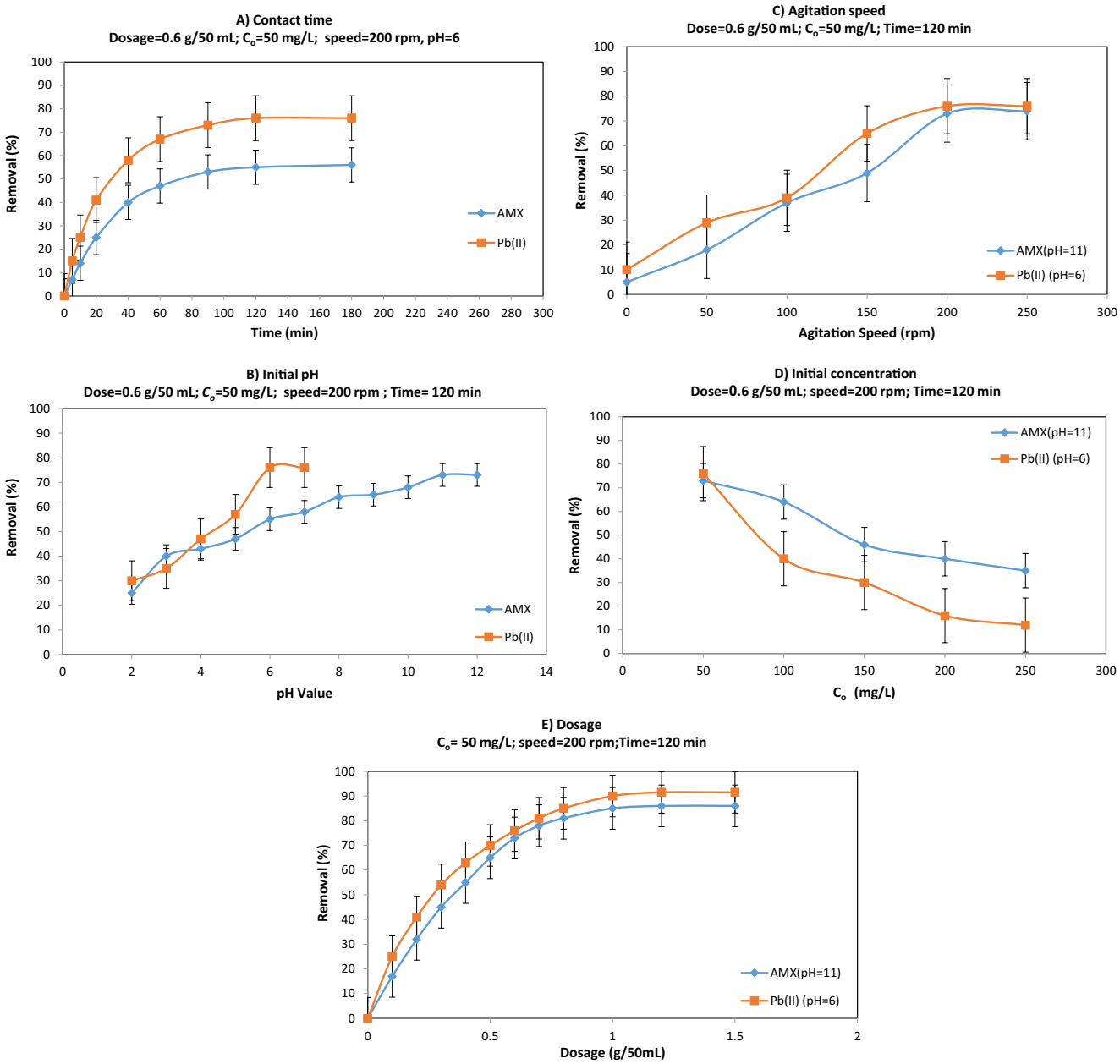

Fig. 6. AMX and Pb(II) percent removal at diverse parameter (A) contact time, (B) pH, (C) agitation speed, (D) initial concentration, and (E) dosage of S-Fe/Zn.

removal efficiency. These findings are consistent with previous research conducted by other researchers [49,50] which also observed a saturation point in the removal efficiency with increasing sorbent dosage. This information is valuable for optimizing the dosage of S-Fe/Zn composite in practical applications, ensuring efficient removal of AMX and Pb(II) while minimizing the amount of sorbent material used and associated costs.

3.3. Sorption isotherm

In the sorption tests, the interaction of S-Fe/Zn with AMX and Pb(II) was analyzed using isotherm models. The equilibrium results were obtained, and the parameters for these models are presented in Table 1. The experimental data were compared with the isotherm models, as shown in Fig. 7. Based on the comparison, it can be observed that the Freundlich model exhibited a higher coefficient of determination (R^2) compared to the Langmuir model. This indicates that the Freundlich model provides a better fit to the experimental data and more accurately describes the sorption process of AMX and Pb(II) onto S-Fe/Zn. The higher R^2 value suggests that the sorption of AMX and Pb(II) involves the binding of multiple molecular layers on the surface of S-Fe/Zn. The Freundlich model is commonly used to describe sorption onto heterogeneous surfaces and

assumes that the sorption occurs on sites with different affinities and energies. It accounts for non-ideal sorption behavior and suggests that the sorption capacity increases with increasing concentration of the sorbate. It can be noted that the maximum adsorption capacity of the prepared nanocomposite (S-Fe/Zn) was 5.662 and 8.854 mg/g for AMX and Pb(II), respectively, as presented in Table 1. These findings support the applicability of using S-Fe/Zn as a sorbent for the removal of AMX and Pb(II) from aqueous solutions, in comparison with other sorbent materials that were used in previous works, as illustrated in Table 2.

Table 1
Parameters resulted from fitting of equilibrium isotherm measurements for sorption of Pb(II) and AMX

Model	Parameter	Pb(II)	AMX
Freundlich	K_F, (mg/g)(L/mg)$^{1/n}$	0.964	0.868
	n	1.898	2.238
	R^2	0.996	0.978
	SSE	0.087	0.204
Langmuir	q_m, (mg/g)	8.854	5.662
	b, (L/mg)	0.061	0.078
	R^2	0.977	0.956
	SSE	0.646	0.424

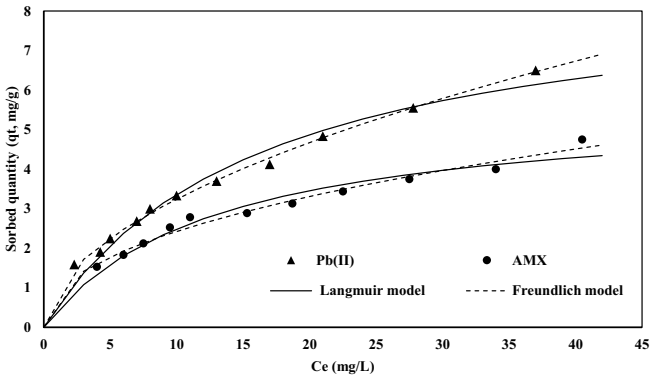

Fig. 7. Isotherm models for sorption of AMX and Pb(II) on S-Fe/Zn nanocomposite.

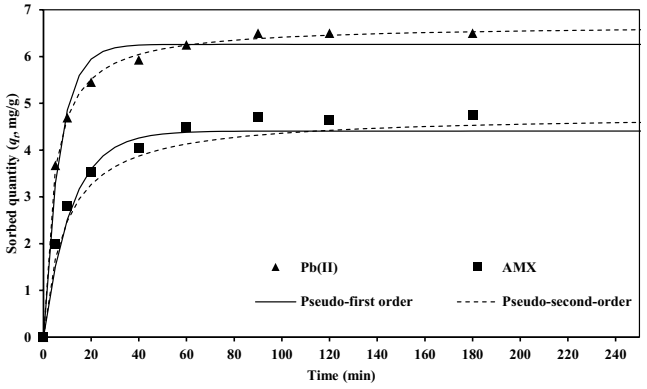

Fig. 8. Models of kinetic and experimental measurements for sorption of AMX and Pb(II).

3.4. Sorption kinetic

Based on the analysis presented in the provided information, the sorption kinetics of AMX and Pb(II) onto the S-Fe/Zn nanocomposite were investigated using pseudo-first-order, pseudo-second-order, and intraparticle diffusion models, as illustrated in Figs. 8 and 9. The experimental data were fitted to these models using Microsoft Excel 2016, and the parameters, determination coefficients (R^2), and sum of squares error (SSE) values are presented in Table 3. Among the kinetic models tested, the pseudo-second-order model demonstrated the value of $q_{e(\text{Theoretical})}$ was closest to the $q_{e(\text{Experimental})}$ with the highest R^2 values and the lowest SSE values, indicating that it is well-suited to describe the sorption kinetics of AMX and Pb(II) onto the S-Fe/Zn nanocomposite. This suggests that the sorption

Table 2
Comparison of the adsorption capacity of prepared nanocomposite with other materials

Sorbent	Adsorption capacity (mg/g)		References
	Pb(II)	AMX	
Carbon nanotubes	12.41	–	[51]
Banana peel	2.18	–	[52]
Activated carbon	–	4.4	[53]
Bean husk	0.9895	–	[54]
Eucalyptus camaldulensis bio-sorbent	9.259	–	[55]
Iron-slag	2.309	–	[56]
Zeolite pellets	4.45	–	[57]
Graphene oxide poly(carboxymethyl cellulose-co-acrylic acid) hydrogel	–	12.48	[58]
Silver nano-based adsorbents	–	3.14	[59]
Calcium/iron-layered double hydroxides-sodium alginate	–	6.73	[60]
Modified bentonite with tetramethylammonium bromide (NB-TMAB)	–	13.73	[39]
S-Fe/Zn nanocomposite	8.854	5.662	(Current study)

Table 3
Resulted parameters of fitting kinetic measurements for sorption of AMX and Pb(II) onto S-Fe/Zn

Model	Parameter	Pb(II)	AMX
Pseudo-first-order	$q_{e(Experimental)}$, (mg/g)	6.5	4.75
	$q_{e(Theoretical)}$, (mg/g)	6.260	4.407
	k_1, (min^{-1})	0.150	0.085
	R^2	0.916	0.981
	SSE	0.685	0.457
Pseudo-second-order	$q_{e(Experimental)}$, (mg/g)	6.5	4.75
	$q_{e(Theoretical)}$, (mg/g)	6.684	4.760
	k_2, (g/mg·min)	0.035	0.023
	R^2	0.995	0.997
	SSE	0.037	0.151
Intraparticle diffusion	Portion 1		
	k_{int}, (mg/g·$min^{0.5}$)	1.2532	0.8055
	R^2	0.9547	0.9892
	Portion 2		
	k_{int}, (mg/g·$min^{0.5}$)	0.2107	0.2394
	R^2	0.9825	0.9656
	Portion 3		
	k_{int}, (mg/g·$min^{0.5}$)	0.0342	0.0156
	R^2	0.6157	0.3843

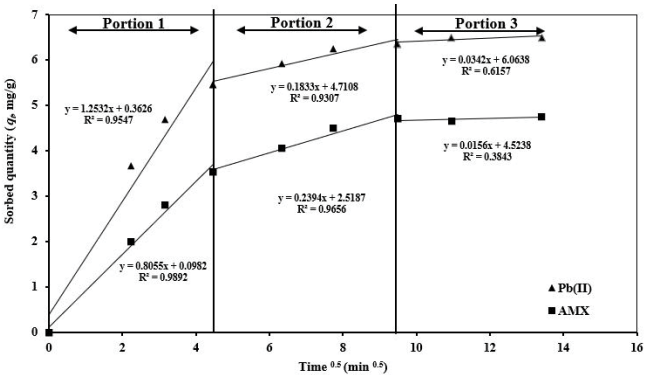

Fig. 9. Model of diffusion through intraparticle for interaction of S-Fe/Zn with the AMX and Pb(II).

process of AMX and Pb(II) involves chemisorption, where the adsorbate molecules are strongly bound to the adsorbent surface. Furthermore, the intraparticle diffusion model was applied to examine the sorption kinetics and the relationship between the half-time ($t^{0.5}$) and the amount of adsorbate (q_t). The linear relationships with acceptable R^2 values depicted in Fig. 9 indicated that intraparticle diffusion plays a role in the sorption process of AMX and Pb(II), although it is not the rate-controlling step. The intraparticle diffusion model analysis revealed three sections of linearity, indicating the presence of multiple steps in the sorption process. The rate constants (k_{int}) for these sections were determined, with higher values observed for "portion 1" compared to "portions 2 and 3". This suggests that the initial portion is influenced by prompt or external surface sorption, while

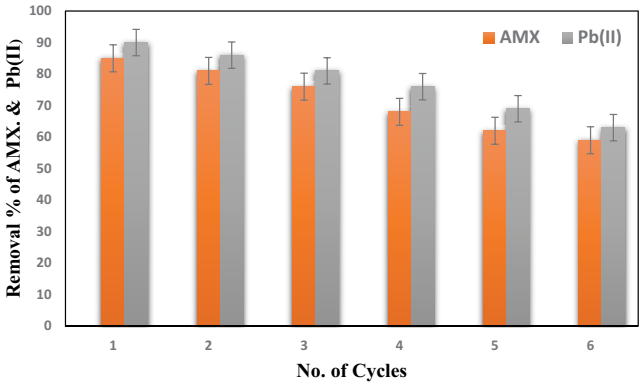

Fig. 10. Reusability of S-Fe/Zn for removal of AMX and Pb(II) for many cycles.

the subsequent portions involve other mechanisms, such as intraparticle diffusion [37]. The presence of three main steps (bulk diffusion, intraparticle diffusion, and equilibrium) in the sorption processes of AMX and Pb(II) on the S-Fe/Zn nanocomposite was identified based on the analysis. The diffusion of pores and films, as well as macro pore diffusion, were proposed to play significant roles in the sorbent. Overall, the findings indicate that both diffusion and external mass transfer contribute to the sorption process, with intraparticle diffusion playing a role in the overall kinetics [57]. The data analysis provides valuable insights into the sorption mechanisms and can aid in optimizing the sorption process for the removal of AMX and Pb(II) using the S-Fe/Zn nanocomposite.

3.5. Reusability of S-Fe/Zn nanocomposite

The reusability test conducted on the S-Fe/Zn nanocomposite involved subjecting the composite to multiple cycles of interaction with AMX and Pb(II) solutions. The composite was reused for a total of five cycles under the optimal conditions determined in previous steps. The results depicted in Fig. 10 show that the removal percentage gradually decreased with each reuse cycle, indicating a decrease in the sorption efficiency over time. This decline in removal percentage can be attributed to the gradual saturation of the active sites on the S-Fe/Zn nanocomposite or possible changes in the composite's surface characteristics after multiple interactions. To confirm the strong bonding between the Fe/Zn nanoparticles and the sand surface, the concentrations of Fe and Zn ions were analyzed in the aqueous solution after all six cycles of reuse. The analysis revealed that the concentration of the Fe/Zn ions leached to the aqueous solution was at a minimal level, less than 0.0003 mg/L even after the sixth cycle, indicating that the nanoparticles (Fe/Zn) remained strongly bonded to the sand surface even after multiple cycles. These findings demonstrate the stability and durability of the S-Fe/Zn composite and its ability to retain the nanoparticles on the sand surface during the sorption process. Based on the information provided, the creation of bimetallic nanoparticles on sand using the S-Fe/Zn composite can be considered a highly advantageous and environmentally responsible approach. The strong bonding between the nanoparticles and the sand surface, coupled with the

composite's effectiveness in removing AMX and Pb(II), makes it a promising and sustainable option for wastewater treatment or other applications requiring pollutant removal.

4. Conclusion

The synthesis of the S-Fe/Zn nanocomposite was achieved through a green method that avoids the use of toxic chemicals, ensuring minimal adverse effects on the environment. The composite exhibited effective removal capabilities for both organic (AMX) and inorganic (Pb(II)) contaminants through batch processes. Several parameters were investigated to understand their influence on the removal of AMX and Pb(II). The optimized values for these parameters were determined as follows: contact time of 120 min, initial pH of 11 for AMX and 6 for Pb(II), agitation speed of 200 rpm, initial concentration of 50 mg/L, and S-Fe/Pb dosage of 1 g/50 mL, to be effective in achieving the maximum removal percentage of 90% for Pb(II) and 85% for AMX with a maximum sorption capacity of 8.854 and 5.662 mg/g for Pb(II) and AMX, respectively. The batch experimental results demonstrated that the sorption data for AMX and Pb(II) could be accurately described by the Freundlich isotherm model, indicating multi-molecular layer sorption on the composite surface. From a kinetic perspective, the pseudo-second-order model provided the best fit to the experimental data, indicating that the sorption of AMX and Pb(II) followed chemisorption kinetics. Additionally, the intraparticle diffusion model revealed that external mass transfer played a significant role in the sorption process, while diffusion controlled the rate of sorption. In conclusion, the synthesis of the S-Fe/Zn nanocomposite using a green method offers a promising and environmentally friendly approach. The composite demonstrates efficient removal of AMX and Pb(II) from aqueous solutions. The results suggest that the application of prepared bimetallic nanocomposite for the removal of contaminants from the aqueous solutions provides a sustainable solution for water treatment and pollution remediation.

References

[1] N.A. Abdulhusain, Z.T. Abd Ali, Green synthesis of sand-bimetallic Fe/Pb nanoparticles as an environmentally sustainable composite for ciprofloxacin and copper removal from aqueous solutions, Desal. Water Treat., 287 (2023) 155–166.

[2] B.H. Graimed, Z.T. Abd Ali, Thermodynamic and kinetic study of the adsorption of Pb(II) from aqueous solution using bentonite and activated carbon, Al-Khwarizmi Eng. J., 9 (2013) 48–56.

[3] M.A. Atiya, A.K. Hassan, F.Q. Kadhim, Green synthesis of copper nanoparticles using tea leaves extract to remove ciprofloxacin (CIP) from aqueous media, Iraqi J. Sci., 62 (2021) 2832–2854.

[4] T. Seema, I.P. Tripathi, H.I. Tiwari, Effects of lead on environment, Int. J. Emerging Res. Manage. Technol., 2 (2013) 23–45.

[5] A.F. Ali, Z.T. Abd Ali, Interaction of aqueous Cu^{2+} ions with granules of crushed concrete, Iraqi J. Chem. Pet. Eng., 20 (2019) 31–38.

[6] T.A. Saleh, I. Ali, Synthesis of polyamide grafted carbon microspheres for removal of Rhodamine B dye and heavy metals, J. Environ. Chem. Eng., 6 (2018) 5361–5368.

[7] A.A. Basaleh, M.H. Al-Malack, T.A. Saleh, Poly(acrylamide acrylic acid) grafted on steel slag as an efficient magnetic adsorbent for cationic and anionic dyes, J. Environ. Chem. Eng., 9 (2021) 105126, doi: 10.1016/j.jece.2021.105126.

[8] O. Al-Hashimi, K. Hashim, E. Loffill, T.M. Čebašek, I. Nakouti, A.A.H. Faisal, N. Al-Ansari, A comprehensive review for groundwater contamination and remediation: occurrence, migration and adsorption modelling, Molecules, 26 (2021) 5913, doi: 10.3390/molecules26195913.

[9] R.A. Crane, T.B. Scott, Nanoscale zero-valent iron: future prospects for an emerging water treatment technology, J. Hazard. Mater., 211–212 (2012) 112–125.

[10] G. Gopal, H. Sankar, C. Natarajan, A. Mukherjee, Tetracycline removal using green synthesized bimetallic nZVI-Cu and bentonite supported green nZVI-Cu nanocomposite: a comparative study, J. Environ. Manage., 254 (2020) 109812, doi: 10.1016/j.jenvman.2019.109812.

[11] K.V.G. Ravikumar, S.V. Sudakaran, K. Ravichandran, M. Pulimi, C. Natarajan, A. Mukherjee, Green synthesis of NiFe nano particles using *Punica granatum* peel extract for tetracycline removal, J. Cleaner Prod., 210 (2019) 767–776.

[12] X. Weng, Q. Sun, S. Lin, Z. Chen, M. Megharaj, R. Naidu, Enhancement of catalytic degradation of amoxicillin in aqueous solution using clay supported bimetallic Fe/Ni nanoparticles, Chemosphere, 103 (2014) 80–85.

[13] Z. Chen, X. Jin, Z. Chen, M. Megharaj, R. Naidu, Removal of methyl orange from aqueous solution using bentonite-supported nanoscale zero-valent iron, J. Colloid Interface Sci., 363 (2011) 601–607.

[14] X. Weng, W. Cai, R. Lan, Q. Sun, Z. Chen, Simultaneous removal of amoxicillin, ampicillin and penicillin by clay supported Fe/Ni bimetallic nanoparticles, Environ. Pollut., 236 (2018) 562–569.

[15] B.H. Graimed, Z.T. Abd Ali, Batch and continuous study of one-step sustainable green graphene sand hybrid synthesized from date-syrup for remediation of contaminated groundwater, Alexandria Eng. J., 61 (2022) 8777–8796.

[16] E. González-Burgos, M. Liaudanskas, J. Viškelis, V. Žvikas, V. Janulis, M. Gómez-Serranillos, Antioxidant activity, neuroprotective properties and bioactive constituents analysis of varying polarity extracts from *Eucalyptus globulus* leaves, J. Food Drug Anal., 26 (2018) 1293–1302.

[17] M.G. da Silva, M.A.S. de Barros, R.T.R. de Almeida, E.J. Pilau, E. Pinto, G. Soares, J.G. Santos, Cleaner production of antimicrobial and anti-UV cotton materials through dyeing with *Eucalyptus* leaves extract, J. Cleaner Prod., 199 (2018) 807–816.

[18] C. Acuña-Alonso, O. Lorenzo, X. Álvarez, A. Cancela, E. Valero, A. Sánchez, Influence of *Microcystis* sp. and freshwater algae on pH: changes in their growth associated with sediment, Environ. Pollut., 263 (2020) 114435, doi: 10.1016/j.envpol.2020.114435.

[19] A. Dehghani, G. Bahlakeh, B. Ramezanzadeh, Green *Eucalyptus* leaf extract: a potent source of bio-active corrosion inhibitors for mild steel, Bioelectrochemistry, 130 (2019) 107339, doi: 10.1016/j.bioelechem.2019.107339.

[20] W. Zhao, Z. Zheng, J.L. Zhang, S.-F. Roger, X.Z. Luo, Allelopathically inhibitory effects of *Eucalyptus* extracts on the growth of *Microcystis aeruginosa*, Chemosphere, 225 (2019) 424–433.

[21] Y. Chen, J. Wang, Y. Ou, H. Chen, S. Xiao, G. Liu, Y. Cao, Q. Huang, Cellular antioxidant activities of polyphenols isolated from *Eucalyptus* leaves (*Eucalyptus grandis* × *Eucalyptus urophylla GL9*), J. Funct. Foods, 7 (2014) 737–745.

[22] B. Gullón, A. Muñiz-Mouro, T.A. Lú-Chau, M.T. Moreira, J.M. Lema, G. Eibes, Green approaches for the extraction of antioxidants from *Eucalyptus* leaves, Ind. Crops Prod., 138 (2019) 111473, doi: 10.1016/j.indcrop.2019.111473.

[23] M. Danish, X. Gu, S. Lu, A. Ahmad, M. Naqvi, U. Farooq, Y. Xue, Efficient transformation of trichloroethylene activated through sodium percarbonate using heterogeneous zeolite supported nano zero valent iron-copper bimetallic composite, Chem. Eng. J., 308 (2017) 396–407.

[24] A. Panáček, L. Kvítek, R. Prucek, M. Kolář, R. Večeřová, N. Pizúrová, R. Zbořil, Silver colloid nanoparticles: synthesis, characterization, and their antibacterial activity, J. Phys. Chem. B, 110 (2006) 16248–16253.

[25] A.F. Ali, Z.T. Abd Ali, Sustainable use of concrete demolition waste as reactive material in permeable barrier for remediation of groundwater: batch and continuous study, J. Environ. Eng., 146 (2020) 04020048, doi: 10.1061/(ASCE)EE.1943-7870.0001714.
[26] X. Huang, Y. Zhang, D. Zhang, W. Ding, X. Hu, Reduced graphene oxide supported Fe/Ni bimetallic nanoparticles for the rapid adsorption and dechlorination of 2,4-dichlorophenol, Mater. Today Commun., 35 (2023) 105983, doi: 10.1016/j.mtcomm.2023.105983.
[27] K.V.G. Ravikumar, H. Kubendiran, R. Gupta, A. Gupta, P. Sharma, S.A. Alex, A. Mukherjee, *In-situ* coating of Fe/Pd nanoparticles on sand and its application for removal of tetracycline from aqueous solution, J. Water Process Eng., 36 (2020) 101400, doi: 10.1016/j.jwpe.2020.101400.
[28] N. Arancibia-Miranda, S.E. Baltazar, A. García, D. Muñoz-Lira, P. Sepúlveda, M. Rubio, D. Altbir, Nanoscale zero valent supported by zeolite and montmorillonite: template effect of the removal of lead ion from an aqueous solution, J. Hazard. Mater., 301 (2016) 371–380.
[29] K.V.G. Ravikumar, G. Debayan, P. Mrudula, N. Chandrasekaran, M. Amitava, *In-situ* formation of bimetallic FeNi nanoparticles on sand through green technology: application for tetracycline removal, Front. Environ. Sci. Eng., 14 (2020) 1–13.
[30] B.H. Graimed, Z.T. Abd Ali, Green approach for the synthesis of graphene glass hybrid as a reactive barrier for remediation of groundwater contaminated with lead and tetracycline, Environ. Nanotechnol. Monit. Manage., 18 (2022) 100685, doi: 10.1016/j.enmm.2022.100685.
[31] N.A. Abdulhusain, Z.T. Abd Ali, Green approach for fabrication of sand-bimetallic (Fe/Pb) nanocomposite as reactive material for remediation of contaminated groundwater using permeable reactive barrier, Alexandria Eng. J., 72 (2023) 511–530.
[32] M.N. Ezzat, Z.T. Abd Ali, Green approach for fabrication of graphene from polyethylene terephthalate (PET) bottle waste as reactive material for dyes removal from aqueous solution: batch and continuous study, Sustainable Mater. Technol., 32 (2022) e00404, doi: 10.1016/j.susmat.2022.e00404.
[33] Z.T. Abd Ali, Green synthesis of graphene-coated glass as novel reactive material for remediation of fluoride-contaminated groundwater, Desal. Water Treat., 226 (2021) 113–124.
[34] Z.T. Abd Ali, Green synthesis of graphene-coated sand (GCS) using low-grade dates for evaluation and modeling of the pH-dependent permeable barrier for remediation of groundwater contaminated with copper, Sep. Sci. Technol., 56 (2021) 14–25.
[35] Z.T. Abd Ali, H.J. Khadim, M.A. Ibrahim, Simulation of the remediation of groundwater contaminated with ciprofloxacin using grafted concrete demolition wastes by ATPES as reactive material: batch and modeling study, Egypt. J. Chem., 65 (2022) 1–2.
[36] Z.T. Abd Ali, A comparative isothermal and kinetic study of the adsorption of lead(II) from solution by activated carbon and bentonite, J. Eng., 21 (2015) 45–58.
[37] Z.T. Abd Ali, Combination of the artificial neural network and advection-dispersion equation for modeling of methylene blue dye removal from aqueous solution using olive stones as reactive bed, Desal. Water Treat., 179 (2020) 302–311.
[38] Z.T. Abd Ali, Z.Z. Ismail, Experimental and modeling study of water defluoridation using waste granular brick in a continuous up-flow fixed bed, Environ. Eng. Res., 26 (2021) 190506, doi: 10.4491/eer.2019.506.
[39] A.A. Naji, Z.T. Abd Ali, Evaluation of modified bentonite using chemical and physical methods for removal of amoxicillin from aqueous solutions: batch and continuous study, Desal. Water Treat., 294 (2023) 185–201.
[40] A.H. Sulaymon, Z.T. Abd Ali, Removal of kerosene from wastewater using Iraqi bentonite, J. Eng., 16 (2010) 46–62.
[41] L. Du, L. Luo, Z. Feng, M. Engelhard, X. Xie, B. Han, Y. Shao, Nitrogen–doped graphitized carbon shell encapsulated NiFe nanoparticles: a highly durable oxygen evolution catalyst, Nano Energy, 39 (2017) 245–252.
[42] L. Du, L. Luo, Z. Feng, M. Engelhard, X. Xie, B. Han, Y. Shao, Efficient removal of uranium from aqueous solution by zero-valent iron nanoparticle and its graphene composite, J. Hazard. Mater., 290 (2015) 26–33.
[43] S. Khan, A. Achazhiyath Edathil, F. Banat, Sustainable synthesis of graphene-based adsorbent using date syrup, Sci. Rep., 9 (2019) 18106, doi: 10.1038/s41598-019-54597-x.
[44] S. Kaviya, Rapid naked eye detection of arginine by pomegranate peel extract stabilized gold nanoparticles, J. King Saud Univ., 31 (2019) 864–868.
[45] A.M. Osman, A.H. Hendi, T.A. Saleh, Simultaneous adsorption of dye and toxic metal ions using an interfacially polymerized silica/polyamide nanocomposite: kinetic and thermodynamic studies, J. Mol. Liq., 314 (2020) 113640, doi: 10.1016/j.molliq.2020.113640.
[46] J. Liu, Y. Du, W. Sun, Q. Chang, C. Peng, A granular adsorbent-supported Fe/Ni nanoparticles activating persulfate system for simultaneous adsorption and degradation of ciprofloxacin, Chin. J. Chem. Eng., 28 (2020) 1077–1084.
[47] D. Wang, J. Li, Z. Xu, Y. Zhu, G. Chen, Preparation of novel flower-like $BiVO_4/Bi_2Ti_2O_7/Fe_3O_4$ for simultaneous removal of tetracycline and Cu^{2+}: adsorption and photocatalytic mechanisms, J. Colloid Interface Sci., 533 (2019) 344–357.
[48] R.A. Crane, T. Scott, Simulation of the remediation of groundwater contaminated with ciprofloxacin using grafted concrete demolition wastes by ATPES as reactive material: batch and modeling study, Egypt. J. Chem., 65 (2022) 1–2.
[49] S. Kango, R. Kumar, Magnetite nanoparticles coated sand for arsenic removal from drinking water, Environ. Earth Sci., 75 (2016) 1–12.
[50] T.H. Mhawesh, Z.T. Abd Ali, Reuse of brick waste as a cheap-sorbent for the removal of nickel ions from aqueous solutions, Iraqi J. Chem. Pet. Eng., 21 (2020) 15–23.
[51] Y.H. Li, Z. Di, D. Wu, Z. Luan, Y. Zhu, Adsorption thermodynamic, kinetic and desorption studies of Pb^{2+} on carbon nanotubes, Water Res., 39 (2005) 605–609.
[52] J. Anwar, U. Shafique, M. Salman, A. Dar, S. Anwar, Removal of Pb(II) and Cd(II) from water by adsorption on peels of banana, Bioresour. Technol., 101 (2010) 1752–1755.
[53] M.A.E. de Franco, C.B. de Carvalho, M.M. Bonetto, R. de Pelegrini Soares, L.A. Féris, Removal of amoxicillin from water by adsorption onto activated carbon in batch process and fixed bed column: kinetics, isotherms, experimental design and breakthrough curves modelling, J. Cleaner Prod., 161 (2017) 947–956.
[54] C.T. Onwordi, C.C. Uche, A.E. Ameh, L.F. Petrik, Comparative study of the adsorption capacity of lead(II) ions onto bean husk and fish scale from aqueous solution, J. Water Reuse Desal., 9 (2019) 249–262.
[55] H. Gebretsadik, A. Gebrekidan, L. Demlie, Removal of heavy metals from aqueous solutions using *Eucalyptus camaldulensis*: an alternate low-cost adsorbent, Cogent Chem., 6 (2020) 1720892, doi: 10.1080/23312009.2020.1720892.
[56] S.S. Alquzweeni, A.A. Faisal, Possibility of using granular iron slag by-product as permeable reactive barrier for remediation of simulated water contaminated with lead ions, Desal. Water Treat., 178 (2020) 211–219.
[57] Z.B. Masood, Z.T. Abd Ali, Numerical modeling of two-dimensional simulation of groundwater protection from lead using different sorbents in permeable barriers, Environ. Eng. Res., 25 (2020) 605–613.
[58] M.A. Awad, A.M. Kadhum, S.H. Mallah, Synthesis and characterization of C/ZnO nanocomposite: adsorption isotherm of a reactive green from aqueous solutions, NeuroQuantolog, 19 (2021) 96–103.
[59] O.B. Omitola, M.N. Abonyi, K.G. Akpomie, F.A. Dawodu, Adams–Bohart, Yoon–Nelson, and Thomas modeling of the fix-bed continuous column adsorption of amoxicillin onto silver nanoparticle-maize leaf composite, Appl. Water Sci., 12 (2022) 94, doi: 10.1007/s13201-022-01624-4.
[60] M.F. Abed, A.A. Faisal, Green synthesis of calcium/iron-layered double hydroxides-sodium alginate nano adsorbent as reactive barrier for antibiotic amoxicillin removal from groundwater, Adsorpt. Sci. Technol., 2023 (2023) 1475278, doi: 10.1155/2023/1475278.